A Tensor Residual Circuit Neural Network Factorized with Matrix Product Operation

Andi Chen

Abstract

It is challenging to reduce the complexity of neural networks while maintaining their generalization ability and robustness, especially for practical applications. Conventional solutions for this problem incorporate quantum-inspired neural networks with Kronecker products and hybrid tensor neural networks with MPO factorization and fully-connected layers. Nonetheless, the generalization power and robustness of the fullyconnected layers are not as outstanding as circuit models in quantum computing. In this paper, we propose a novel tensor circuit neural network (TCNN) that takes advantage of the characteristics of tensor neural networks and residual circuit models to achieve generalization ability and robustness with low complexity. The proposed activation operation and parallelism of the circuit in complex number field improves its non-linearity and efficiency for feature learning. Moreover, since the feature information exists in the parameters in both the real and imaginary parts in TCNN, an information fusion layer is proposed for merging features stored in those parameters to enhance the generalization capability. Experimental results confirm that TCNN showcases more outstanding generalization and robustness with its average accuracies on various datasets 2%-3% higher than those of the state-of-the-art compared models. More significantly, while other models fail to learn features under noise parameter attacking, TCNN still showcases prominent learning capability owing to its ability to prevent gradient explosion. Furthermore, it is comparable to the compared models on the number of trainable parameters and the CPU running time. An ablation study also indicates the advantage of the activation operation, the parallelism architecture and the information fusion layer.

Introduction

With the rapid development of neural networks and tensor networks, tensor neural network, a neural network designed to process tensor data directly, leverages the multidimensional structures of tensors to capture complex features (Buduma, Buduma, and Papa 2022; Li et al. 2021; Wang et al. 2023; Chien and Bao 2017; Yin et al. 2022;

Copyright © 2026, Association for the Advancement of Artificial Intelligence (www.aaai.org). All rights reserved.

Hameed et al. 2022; Ouerfelli, Tamaazousti, and Rivasseau 2022; Zhou, Han, and Yu 2025). By matrix factorization and decomposition, it usually possesses fewer trainable parameters and consume fewer resources than classical neural networks with large-sized hidden layers (Bañuls 2023; Fishman, White, and Stoudenmire 2022; Evenbly 2017; Zheng et al. 2021a; Ouerfelli, Tamaazousti, and Rivasseau 2022; Hameed et al. 2022). Nevertheless, one problem lies in its limited generalization power and robustness due to its small parameter manifold spaces, which implies that their capability of pattern learning and interference resistance requires to be further facilitated (Wang et al. 2023). Meanwhile, in quantum computing, residual circuit model demonstrates outstanding fault tolerance, high fidelity and strong generalization and robustness for feature extraction based on their logical unitary gates on the quantum-inspired deep learning field (Chiribella, D'Ariano, and Perinotti 2008; Mitarai et al. 2018; Marinov and Neittaanmäki 2012; Chen et al. 2024: Chou et al. 2022: Fan et al. 2024: He et al. 2024: Dos Martires 2024; Rudolph et al. 2023). Nevertheless, owing to continuous multiplications of sparse matrices, the time complexity of circuit models, usually proportional to the exponential power of the neural network width, is relatively higher than that of classical neural networks (Goodfellow, Bengio, and Courville 2016; Chen et al. 2024; Yao 2024; Rudolph et al. 2023).

Hence, to improve the generalization power, robustness while reducing complexity of feedforward neural networks in the meantime, in this paper, we propose a Tensor Circuit Neural Network (TCNN) with matrix product operators and residually continuous circuit architecture. Clean, enhanced and noisy MNIST, FASHIONMNIST, CIFAR, ImageNet and CelebA datasets are for the assessment of generalization capability and robustness of TCNN (Deng 2012; Xiao, Rasul, and Vollgraf 2017; Shin et al. 2016; Hendrycks et al. 2021; Hendrycks and Dietterich 2019). Besides that, we also select another several state-of-theart feedforward neural networks incorporating a Multi-Layer Perceptron (MLP), a Hybrid Feedforward Tensor Neural Network (HFTNN) (Wang et al. 2023), a Hybrid Feedforward Circuit Neural Network (HFCNN) (Chen et al. 2024), a Quantum-inspired Multi-Layer Perceptron (QiMLP) (Zhang et al. 2025), a Factor Augmented Tensoron-Tensor Neural Network (FATTNN)(Zhou, Han, and Yu 2025), a Hybrid Quantum-classical convolutional Network (HQNet)(Wang et al. 2025), a residual and a dense convolutional neural networks with spatial and channel attentions (Resnet and Densenet) (Hameed et al. 2022) for model comparison. Experiments demonstrate that TCNN possess benefits on complexity, generalization capability, robustness and stability. Hence, the contributions in this paper are as follows:

- We devise a tensor circuit neural network that is comprised of a tensor network with MPO factorization with paralleled adaptive residual circuit framework in complex number field;
- The parameter complexity of TCNN is lower than or comparable to that of the compared models;
- Experiments showcase that our TCNN is more advantageous than all the compared models on generalization power and accuracy on image recognition.
- Experiments indicate that our TCNN showcases much more outstanding robustness to random noise parameter attacks than all the compared models. The reason lies in the strong capability of it to prevent gradient explosion.

Related work

Tensor neural networks. In tensor neural networks, through various decomposition methods, high-dimensional matrices could be decomposed into low-dimensional parameterized tensors that possess learning capability and are stored in lists or tuples without taking up too much resource. Common methods incorporate Block-Term Tucker (BTT) decomposition, Matrix Product State (MPS) decomposition, Tensor Train (TT) decomposition, Matrix Product Operator (MPO) factorization, etc. while other methods need to solve the eigenvalues or singular values, MPO factorization, allowing parallel computation of local tensor operations, is more efficient without computing those values (Neill 2020; Zheng et al. 2021b; Zhou, Han, and Yu 2025; Ouerfelli, Tamaazousti, and Rivasseau 2022; Hameed et al. 2022; Panagakis et al. 2021). Compared with Kronecker method, it saves more time with strong explainability (Gao et al. 2020; Zhou, Han, and Yu 2025). Hence, impacted by MPO method for compressing deep neural networks (Gao et al. 2020), we utilize an MPO factorization by constituting several small-sized activated parameter matrices for feature learning, which may also reduce the number of trainable parameters and save training and testing time.

Residual circuit models. As is shown on fig.1, through direct linear addition between adjacent layers $H_{h-1}(x)$ and $H_h(x)$, the residual network effectively transfers the main features in the data forward, thereby improving the accuracy and generalization ability. Hence, some works have explored the performance of residual circuit models that are capable of both capturing data patterns and preventing gradient explosion, which improves their ability of resisting noise interferences (Chen et al. 2024; Chou et al. 2022; Noh, Jeong, and Hwang 2025; Liang et al. 2021; Kashif and Al-Kuwari 2024). However, in these works, the circuit model only represents linear mapping and possess serial architectures. And most of them don't involve complex number. Si-

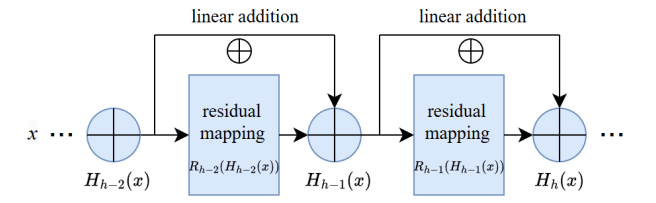


Figure 1: Residual connections. As for the proposed residual circuit model in this paper, the residual mapping is continuous unitary transformation with activations.

multaneously, a few works demonstrate that paralleled circuit networks and complex neural networks are able to capture patterns with different details, thus improving generalization power (Goodfellow, Bengio, and Courville 2016; He et al. 2024; Heidari, Grama, and Szpankowski 2022; Li et al. 2025; Dos Martires 2024). Therefore, we propose parallel non-linear circuit models with activations in complex number field, which may further assist to capture important data features develop neural networks in complex number field.

Preliminaries

Matrix product operator factorization. Suppose N_x and N_y are respectively the dimensions of X and Y. To construct the factorized matrices of the MPO method, we firstly reshape W into a 2n-indexed tensor:

$$W = W_{j_1 j_2 \dots j_n, i_1 i_2 \dots i_n}. (1)$$

Here, the one-dimensional input X with dimension N_x is reshaped into a tensor of n order, X_{i_1,i_2,\ldots,i_n} , with the index of the k^{th} order being $i_k(k=1,2,\ldots n)$. In the meantime, the one-dimensional output Y with dimension N_y is reshaped into a tensor of n order Y_{j_1,j_2,\ldots,j_n} as well, with the index of the k^{th} order being $j_k(k=1,2,\ldots n)$. Suppose I_k and J_k are the dimensions of i_k and j_k separately, we have:

$$\prod_{k=1}^{n} I_k = N_x, \ \prod_{k=1}^{n} J_k = N_y.$$
 (2)

Besides that, the total number of trainable parameters in the MPO factorization process, P_{MPO} , is:

$$P_{MPO} = \prod_{k=2}^{n-1} (I_k J_k D^2) + (I_1 J_1 + I_n J_n) D + N_y$$
 (3)

Circuit evolution. In our framework, the k^{th} evolution process stands for the manipulation to the vector with continuous unitary operations (Chen et al. 2024):

$$O_{k+1} = U_k O_k \quad (k \in \mathbb{N}^+), \tag{4}$$

where U_k represents the k^{th} unitary gate in the k^{th} evolution and O_{k+1} denotes the output vector of the k^{th} evolution. The gate $T_m(\phi_r^l,\theta_r^l)$, frequently utilized in U_k , can be written in

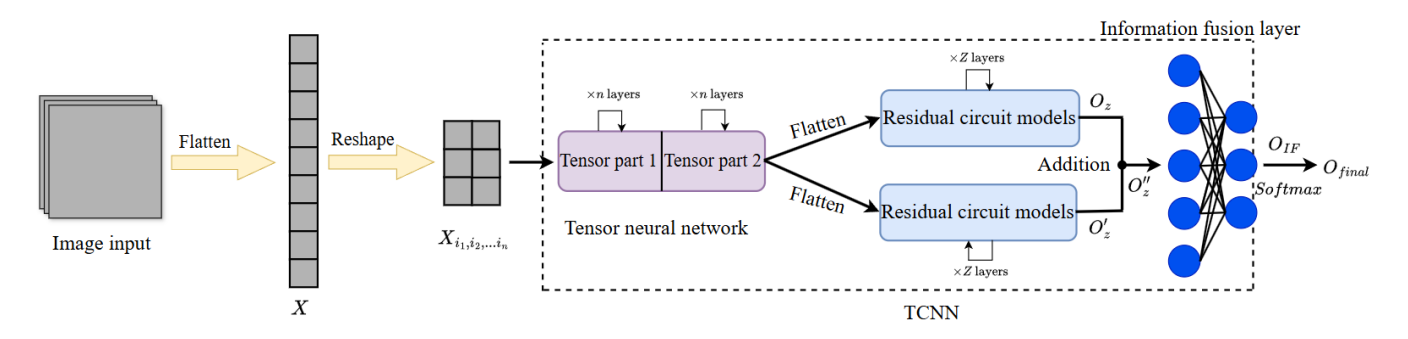


Figure 2: Architecture of TCNN and the process of transferring data into TCNN. TCNN incorporates one tensor neural network architecture with two tensor parts and paralleled circuit framework.

Table 1: Number of trainable parameters in all the models

MLP	QiMLP	FATTNN	HQNet	HFTNN	HFCNN	TCNN
2.67×10^{5}	1.72×10^3	5.58×10^3	2.36×10^3	4.11×10^3	2.02×10^5	4.09×10^{3}

the computational basis as the following matrix

As for this matrix, m denotes the row index of the term $-\sin(\theta_r^l)$, also the column index of the term $\sin(\theta_r^l)$ ($m \in \mathbb{N}^+$). θ_r^l and ϕ_r^l denote the $(r+1)^{th}$ parameter of the real part and the imaginary part separately in the l^{th} circuit layer $(r \in \mathbb{N}, l \in \mathbb{N}^+)$. i represents the imaginary unit. And the relation between r and m is given by:

$$r = \begin{cases} m-1 & 0 \le r \le N-2 \\ 2N-3-m & N-2 < r \le 2N-4, \end{cases} \tag{6}$$

where N is the dimension of the circuit layer.

Methodology

In this section, we illustrate our TCNN which incorporate details of tensor layers and residual circuit layers. Supplementary material shows the frameworks of tensor neural network on the basis of MPO factorization and one layer of the circuit model with unitary evolution and activation. Fig.2 showcases the framework of TCNN comprised of a tensor neural network framework and paralleled residual circuit model.

Framework of TCNN. To begin with, the input image data is firstly flattened into a vector X, which is then transferred into the first tensor part with n tensor layers. Additionally, to extract its feature, we reshape X into a n-order tensor

 $X_{i_1,i_2,...,i_n}$. We also set the dimension of the expected output Y and reshape it into another n-order tensor $Y_{j_1,j_2,...,j_n}$. The MPO representation of weight matrix W is gained by factorizing it into n local tensors that are stored in a list as well:

$$W_{j_1j_2...j_n,i_1i_2...i_n} = list(w^{(1)}[j_1,i_1],...,w^{(n)}[j_n,i_n]),$$
(7)

where $w^{(k)}[j_k,i_k]$ is small-sized parameterized local matrices. We also define the MPO bond vector $D_{bond}=(D_0,D_1,...,D_n)$ to link the local tensors in W and we have $w^{(k)}[j_k,i_k]\in\mathbb{R}^{J_kD_k\times I_kD_{k-1}}$ (Gao et al. 2020). For computation convenience, we suppose $D_0=D_n=1$ and $D_k=D(k=1,...,n-1)$, then $w^{(1)}[j_1,i_1]\in\mathbb{R}^{J_1D\times I_1}, w^{(k)}[j_k,i_k]\in\mathbb{R}^{J_kD\times I_kD}(k\neq0,k\neq n), w^{(n)}[j_n,i_n]\in\mathbb{R}^{J_n\times I_nD}$. In the MPO computing process, $X_{i_1,i_2,...,i_n}$ is reshaped into matrices with various sizes many times based on I_k . Suppose $X_{i_1,i_2,...,i_n}=(X^{(1)},X^{(2)},...,X^{(n)})$, where $X^{(k)}$ is the matrix obtained by reconstructing $X_{i_1,i_2,...,i_n}$ for the k^{th} time. And $X^{(1)}\in\mathbb{R}^{I_1\times I_2I_3...I_n}, X^{(k)}\in\mathbb{R}^{I_kD\times J_1...J_{k-1}I_{k+1}...I_n}$. Suppose the output of the k^{th} tensor layer is Y^k , we have:

$$Y^{k} = w^{(k)}[j_{k}, i_{k}]X^{(k)}(k = 1, 2, ..., n).$$
(8)

 $Y^k \in \mathbb{R}^{J_kD \times J_1...J_{k-1}I_{k+1}...I_n} (k \neq n), Y^n \in \mathbb{R}^{J_n \times J_1...J_{n-1}}.$ And we reshape Y^n to be a vector $Y^n_{final} \in \mathbb{R}^{J_1J_2...J_n}$, eventually we get:

$$Y_{final}^{n} = \sigma(Y^{n} + b), \tag{9}$$

where b represents bias. To further reduce the dimension of the output of the first tensor part, we transfer it into the second tensor part with n tensor layers and local weight matrices as well. The final output vector of the second tensor part is transmitted into the first layer of the paralleled circuit models, which is abbreviated as O_1 now. For the circuit model, fig.3 demonstrates the k^{th} circuit layer with its dimension being 4. The "V" shape circuit assists feature

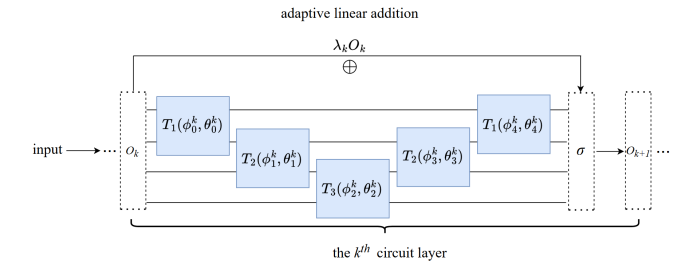


Figure 3: One layer of the residual circuit models with activations. O_k and O_{k+1} separately denote the input and output of the k^{th} circuit layer. σ represents any activation function. ϕ_r^k and θ_r^k represent trainable parameters in the real and imaginary parts. They are updated by back propagation method.

learning avoiding learning imbalance (Chen et al. 2024). The adaptive parameters can effectively control the impact of noise in the data on feature learning (Milletari, Navab, and Ahmadi 2016). We define:

$$U_{k} := \left(\prod_{j=0}^{j=N-2} T_{j+1}(\phi_{j}^{k}, \theta_{j}^{k})\right) \times \left(\prod_{j=N-1}^{j=2N-4} T_{2N-3-j}(\phi_{j}^{k}, \theta_{j}^{k})\right), \tag{10}$$

where U_k is the product of the continuous multiplications of T matrices in the k^{th} circuit layer. Suppose there is Z circuit layers with N dimensions in one circuit model. Then for the output vector of the k^{th} circuit layer of the two paralleled circuits, O_{k+1} and O'_{k+1} , we have:

$$O_{k+1} = \sigma(U_k O_k \oplus \lambda_k O_k)$$

$$O'_{k+1} = \sigma(U'_k O'_k \oplus \lambda'_k O'_k)$$
(11)

where \oplus denotes adaptive residual addition. The formula of U_k' is identical to that of U_k . λ_k and λ_k' are adaptive parameters in the two paralleled circuits. To leverage the upside of the parallelism of circuit models, we transfer two identical O_1 into the two identical circuit models, gaining the output complex vectors of the two circuit models respectively, O_Z and O_Z' . In O_Z , the vectors consisting of the values of the real part of all elements and the values of the imaginary part of all elements are denoted as O_{Z_1} and O_{Z_2} respectively. In O_Z' , the vector consisting of the values of the real part of all elements and the values of the imaginary part of all elements is denoted as O_{Z_1}' and O_{Z_2}' separately. As fig.4 shows, We merge the information of O_{Z_1} and O_{Z_1}' , O_{Z_2} and O_{Z_2}' by linear addition, that is:

$$O_{Z} = O_{Z_{1}} + O_{Z_{2}}i$$

$$O'_{Z} = O'_{Z_{1}} + O'_{Z_{2}}i$$

$$O''_{Z_{1}} = O_{Z_{1}} + O'_{Z_{1}}$$

$$O''_{Z_{2}} = O_{Z_{2}} + O'_{Z_{2}}$$

$$O''_{Z} = concate(O''_{Z_{1}}, O''_{Z_{2}}),$$
(12)

where concate represents concatenation of the two vectors on the column index. $O_{Z_1}^{\prime\prime}$ and $O_{Z_2}^{\prime\prime}$ store different features extracted by the real and imaginary parts of the circuit

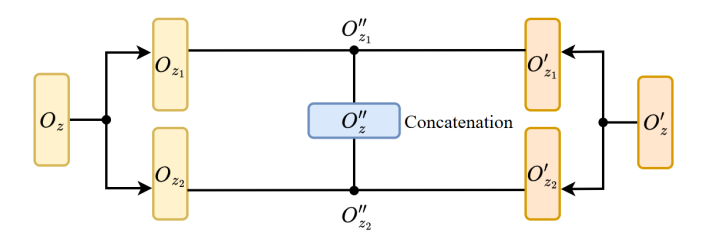


Figure 4: Process of merging information of the real and imaginary parts of the paralleled circuit in the information fusion layer.

models respectively. i is the complex number unit. Then to capture the important patterns in the two vectors, they are concatenated before transferred into the information fusion layer with fully-connected frameworks. We have:

$$O_{IF} = \sigma(W_{IF} \cdot O_z'' + B_{IF})$$

$$O_{final} = softmax(W_{out} \cdot O_{IF} + B_{out}),$$
(13)

where W_{IF} and B_{IF} are weights and biases in the information fusion layer, W_{out} and B_{out} are weights and biases in the output layer. softmax is the softmax activation function of the output layer (Goodfellow, Bengio, and Courville 2016). O_{IF} and O_{final} are the output of the information fusion layer and the output layer separately.

Gradient descent method in complex number field. Some studies have demonstrated gradient descent method in complex number field with various methods such as enhanced gradient descent with Hessian matrices, measurement gradient descent with observables and differential gradient descent (Stokes et al. 2020; Popa 2014; Ji et al. 2024). Contemplating the complexity and convenience, we utilize stochastic gradient descent (SGD) method with momentum to update parameters in the real and imaginary parts in our TCNN. Suppose loss denotes the loss function of our TCNN, for θ_r^k and ϕ_r^k in the k^{th} layer of which the output is O_{k+1} , we have:

$$v_{t} = m_{c}v_{t-1} + (1 - m_{c})\frac{\partial(loss)}{\partial\theta_{r}^{k}}$$

$$v'_{t} = m_{c}v'_{t-1} + (1 - m_{c})\frac{\partial(loss)}{\partial\phi_{r}^{k}}$$

$$\theta_{r}^{k} \leftarrow \theta_{r}^{k} - \eta v_{t}$$

$$\phi_{r}^{k} \leftarrow \phi_{r}^{k} - \eta v'_{t},$$

$$(14)$$

where v_t and v_t' are the momentum factors for the t^{th} update of θ_r^k and ϕ_r^k separately. m_c and η are the momentum coefficient and learning rate respectively. from Eq.(11), we could compute $\frac{\partial O_{(k+1)}}{\partial U_k}$, $\frac{\partial O_{(k+1)}}{\partial O_k}$. From the chain rule (Goodfellow, Bengio, and Courville 2016), we have:

$$\frac{\partial (loss)}{\partial O_Z} = \frac{\partial (loss)}{\partial O_{final}} \cdot \frac{\partial O_{final}}{\partial O_{IF}} \cdot \frac{\partial O_{IF}}{\partial O_Z''} \cdot \frac{\partial O_Z''}{\partial O_Z}$$
(15)

According to Eq.(6), there are two occasions of the derivative of O_{k+1} to the parameters. When $0 \le r \le N-2$, we

also have:

$$\frac{\partial U_k}{\partial \theta_r^k} = \left(\prod_{j=0}^{r-1} T_{j+1}(\phi_j^k, \theta_j^k)\right) \cdot G_{r+1}(\theta_r^k) \cdot \left(\prod_{j=r+1}^{N-2} T_{j+1}(\phi_j^k, \theta_j^k)\right)
\cdot \left(\prod_{j=N-1}^{2N-4} T_{2N-3-j}(\phi_j^k, \theta_j^k)\right)$$
(16a)
$$\frac{\partial U_k}{\partial \phi_r^k} = \left(\prod_{j=0}^{r-1} T_{j+1}(\phi_j^k, \theta_j^k)\right) \cdot G_{r+1}(\phi_r^k) \cdot \left(\prod_{j=r+1}^{N-2} T_{j+1}(\phi_j^k, \theta_j^k)\right)
\cdot \left(\prod_{j=N-1}^{2N-4} T_{2N-3-j}(\phi_j^k, \theta_j^k)\right),$$
(16b)

where $G_{r+1}(\theta_r^k)$ and $G_{r+1}(\phi_r^k)$ are the first derivative matrices of θ_r^k and ϕ_r^k respectively. And when $N-2 < r \le 2N-4$, we have:

$$\frac{\partial U_k}{\partial \theta_r^k} = \left(\prod_{j=0}^{N-2} T_{j+1}(\phi_j^k, \theta_j^k)\right) \cdot \left(\prod_{j=N-1}^{r-1} T_{2N-3-j}(\phi_j^k, \theta_j^k)\right)
\cdot G_{2N-r-3}(\theta_r^k) \cdot \left(\prod_{j=r+1}^{2N-4} T_{2N-3-j}(\phi_j^k, \theta_j^k)\right)
\frac{\partial U_k}{\partial \phi_r^k} = \left(\prod_{j=0}^{N-2} T_{j+1}(\phi_j^k, \theta_j^k)\right) \cdot \left(\prod_{j=N-1}^{r-1} T_{2N-3-j}(\phi_j^k, \theta_j^k)\right)
\cdot G_{2N-r-3}(\phi_r^k) \cdot \left(\prod_{j=r+1}^{2N-4} T_{2N-3-j}(\phi_j^k, \theta_j^k)\right)$$
(17b)

Therefore, the derivative of the loss function to the parameters can be written as:

$$\frac{\partial(loss)}{\partial \theta_r^k} = \frac{\partial(loss)}{\partial O_Z} \cdot (\prod_{j=Z}^{k+2} \frac{\partial O_j}{\partial O_{j-1}}) \cdot \frac{\partial O_{k+1}}{\partial U_k} \cdot \frac{\partial U_k}{\partial \theta_r^k}
(18a)$$

$$\frac{\partial(loss)}{\partial \phi_r^k} = \frac{\partial(loss)}{\partial O_Z} \cdot (\prod_{j=Z}^{k+2} \frac{\partial O_j}{\partial O_{j-1}}) \cdot \frac{\partial O_{k+1}}{\partial U_k} \cdot \frac{\partial U_k}{\partial \phi_r^k},
(18b)$$

According to previous work (Chen et al. 2024), most of the terms in Eq.(18a) and (18b) involve plenty of cosine and sine functions. Due to their limited value range, the derivatives are not very large, thus preventing gradient explosion systematically, while other neural networks don't possess this capability. Besides that, a common problem in circuit model is gradient disappearance (Rudolph et al. 2023). Nevertheless, since residual connection could prevent zero gradient (Goodfellow, Bengio, and Courville 2016), it is relatively easy to train the forward and back propagation of our TCNN. What's more, the update law of parameters in the tensor neural network and another circuit model is similar with that in the circuit model example.

Parameter complexity. Parameter complexity incorporates the parameters that are temporarily stored in each epoch and stored throughout the training and testing processes. According to previous work ((de Sousa Ribeiro and Leite 2021; Chen et al. 2024)), we deduce the parameter complexity of

the circuit model P_{CM} separately contemplating the parameters that could store key information of data features. We have:

$$P_{CM} = O(2Z \cdot (2N - 3)) + O(2Z \cdot (2N - 4))$$

$$+ O(Z - 1) + O(Z - 2)$$

$$\approx O(8NZ)$$

$$\approx O(NZ),$$
(19)

where $O(2Z\cdot(2N-3))$ denotes the number of parameters in the real and imaginary parts in the forward propagation process. $O(2Z\cdot(2N-4))$ denotes the number of the gradients of the parameters in the real and imaginary parts in the back propagation process. O(Z-1) and O(Z-2) are the number of adaptive parameters and the number of their gradients respectively. As for the fully-connected information fusion layer, suppose the matrix size of it is $P_{IF_1}\times P_{IF_2}$, the parameter complexity of the layer, P_{IF} , is:

$$P_{IF} = P_{IF_1} \cdot P_{IF_2} \tag{20}$$

For TCNN, the parameter complexity, P_{TCNN} is:

$$P_{TCNN} = P_{MPO} + 2P_{CM} + P_{IF} \tag{21}$$

The formula of parameter complexity of our TCNN is similar with that of the models in the previous work (Chen et al. 2024). Associated with Eq.(3), the parameter complexity of the compared models is given in table 1. Compared with the MLP, FATTNN and HFCNN, we reduce the number of trainable parameters with MPO method and circuit models in TCNN to a certain extent. In the following experiments, we need to verify whether our TCNN possesses strong generalization ability and robustness without too many parameters.

Experiments

We conduct a few groups of experiments with clean, enhanced and noisy datasets. The indicators include accuracy, loss and CPU running time (Zhou 2021). Details of the baselines are in the supplementary material.

Experiment setup. We use Pytorch, single runs and SGD optimizer to accomplish our experiments. As for the enhanced datasets, we set their brightness, contrast, saturation and hue all being random numbers close to 0.5. For the noisy datasets, we add standard normal distribution or uniform noise, which usually occurs in the engineering field (Bies and Howard 2017), into the images to evaluate the robustness of our proposed network. All the results are testing results.

Generalization power test. We implement different groups of experiments with clean and enhanced data. Fig.5 demonstrates the accuracy curves of the four models on MNIST. Table 2 provides the average accuracy, loss values and CPU running time of TCNN and all the compared models. From the tables, we can see that TCNN showcases a little more advantages than other models on accuracy μ and loss. We also calculate the standard deviation of accuracy E_{μ} with the formula (Goodfellow, Bengio, and Courville 2016):

$$E_{\mu} = Z_{score} \times \sqrt{\frac{\mu \cdot (1 - \mu)}{Q}}, \tag{22}$$

Table 2: Average accuracy, loss values and CPU running time of the seven models with clean and enhanced datasets. * means enhanced datasets.

	Dataset	MLP	QiMLP	FATTNN	HQNet	HFTNN	HFCNN	TCNN
Accuracy	MNIST FASHIONMNIST MNIST* FASHIONMNIST* ImageNet CelebA ImageNet* CelebA*	96.62%±0.61% 92.24%±0.90% 97.86%±0.44% 92.08%±0.91% 76.89%±0.98% 91.43%±0.99% 76.45%±0.99% 92.06%±0.95%	98.14%±0.41% 93.64%±0.79% 99.26%±0.37% 93.26%±0.74% 80.03%±0.77% 92.01%±0.92% 79.38%±0.81% 93.16%±0.72%	97.35%±0.49% 92.06%±0.92% 97.56%±0.47% 92.71%±0.83% 78.54%±0.87% 92.00%±0.92% 78.08%±0.88% 92.18%±0.90%	95.85%±0.68% 91.12%±0.95% 96.59%±0.61% 91.79%±0.94% 77.54%±0.91% 92.95%±0.85% 77.99%±0.90%	96.88%±0.60% 91.67%±0.93% 99.01%±0.37% 91.76%±0.92% 76.88%±0.98% 90.88%±0.93% 80.45 %± 0.78 % 91.56%±1.01%	97.31%±0.46% 92.51%±0.88% 97.95%±0.43% 91.89%±0.94% 78.90%±0.86% 91.91%±0.97% 77.12%±0.96% 91.11%±1.08%	
Loss	MNIST FASHIONMNIST MNIST* FASHIONMNIST* ImageNet CelebA ImageNet* CelebA*	0.0038 0.0076 0.0036 0.0069 0.0849 0.0134 0.0889 0.0189	0.0026 0.0064 0.0024 0.0071 0.0826 0.0103 0.0875 0.0157	0.0031 0.0069 0.0028 0.0073 0.0815 0.0199 0.0846 0.0195	0.0039 0.0078 0.0039 0.0078 0.0857 0.0173 0.0887 0.0157	0.0021 0.0065 0.0029 0.0073 0.0896 0.0134 0.0837 0.0166	0.0024 0.0068 0.0026 0.0070 0.0740 0.0188 0.0804 0.0177	0.0022 0.0062 0.0024 0.0068 0.0727 0.0141 0.0802 0.0150
CPU running time	MNIST FASHIONMNIST MNIST* FASHIONMNIST*	612s 692s 698s 685s	394s 476s 489s 430s	513s 612s 721s 687s	653s 719S 756s 734s	426s 512s 504s 470s	853s 802s 946s 894s	634s 689s 745s 714s

Table 3: Variances of the seven models with enhanced and noisy datasets

Dataset	MLP	QiMLP	FATTNN	HQNet	HFTNN	HFCNN	TCNN
MNIST FASHIONMNIST CIFAR10 CIFAR100 ImageNet CelebA	0.0652	0.0378	0.0390	0.0829	0.0482	0.0977	0.0249
	0.0383	0.0289	0.0531	0.0712	0.0515	0.0417	0.0204
	0.1076	0.0631	0.0865	0.0942	0.1086	0.0689	0.0582
	0.0946	0.0478	0.0745	0.0834	0.0825	0.0792	0.0429
	0.1653	0.1197	0.1245	0.1608	0.1466	0.1551	0.1164
	0.0675	0.0419	0.0501	0.0665	0.0496	0.0592	0.0405

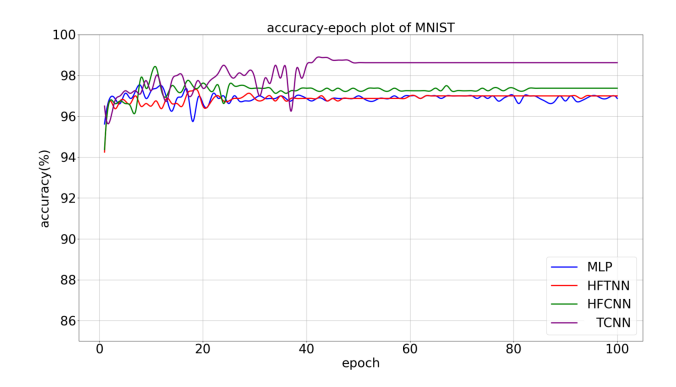


Figure 5: Accuracy curves of the four models on clean MNIST data. All the curves fluctuate first, and then reach convergence. The accuracy of TCNN is the highest.

where Q represents the number of samples in the testing dataset. Considering the 95% confidential intervals, $Z_{score}=1.96$ (Goodfellow, Bengio, and Courville 2016). What's more, the loss values of TCNN are almost the lowest among the compared models. In comparison with HFTNN, the paralleled circuit models in TCNN facilitate generalization capability of it. In contrast with the MLP and HFCNN, TCNN possess lower parameter complexity. Simultaneously, the time complexity of TCNN is comparable to the state-of-the-art MLP and FATTNN, which is lower than that of HFCNN and HQNet. More outcomes in comparison with Resnet and Densenet are in the supplementary material that also demonstrate the advantages of TCNN.

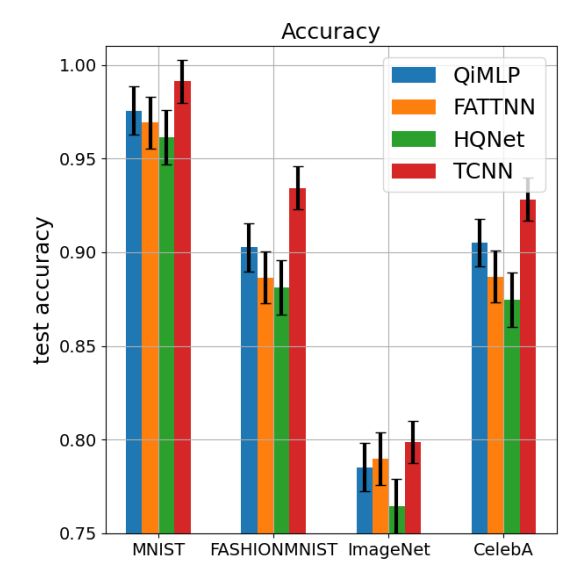


Figure 6: Accuracy charts of the four models on assorted datasets. The accuracy of TCNN is the highest.

Robustness test. Fig.6 demonstrates the accuracy of the four models on datasets with random normal distribution noise. Other results in the supplementary material demonstrate the accuracy, loss values and CPU running time of the compared models. They demonstrate that the learning ability of TCNN is marginally stronger than the other three models according to accuracy and loss values.

Table 4: Accuracy of the seven models to random normal distribution noise attacks

Dataset	MLP	QiMLP	FATTNN	HQNet	HFTNN	HFCNN	TCNN
MNIST FASHIONMNIST							98.86%±1.02% 94.09%±1.39%
CIFAR10	25.00%±2.90%	25.00%±2.90%	25.00%±2.90%	$67.89\% \pm 2.74\%$	25.00%±2.90%	$77.04\% \pm 1.68\%$	$79.54\% \pm 1.38\%$
CIFAR100 ImageNet							76.44%±1.71% 81.02%±1.78%
CelebA							$90.97\% \pm 1.56\%$

Table 5: Loss of the seven models to random normal distribution noise attacks

Dataset	MLP	QiMLP	FATTNN	HQNet	HFTNN	HFCNN	TCNN
MNIST FASHIONMNIST	nan nan	nan nan	nan nan	0.0086 0.0056	nan nan	0.0035 0.0049	0.0024 0.0046
CIFAR10	nan	nan	nan	0.084	nan	0.073	0.046
CIFAR100 ImageNet	nan nan	nan nan	nan nan	0.076 0.123	nan nan	0.056 0.097	0.049 0.078
CelebA	nan	nan	nan	0.085	nan	0.053	0.045

Table 6: Gradients of the loss to a certain attacked parameter of the compared models on CIFAR datasets

noise distribution attack	MLP	QiMLP	FATTNN	HFTNN	Resnet	Densenet
random normal distribution random uniform distribution	nan	nan	nan	nan	nan	nan
	nan	nan	nan	nan	nan	nan

Table 7: Accuracy of the four models. * means enhanced datasets

Dataset	TCNN	TCNN2	TCNN3	TCNN4
MNIST FASHIONMNIST MNIST* FASHIONMNIST* CelebA CelebA*	$\begin{array}{c} 98.95\%\pm1.02\%\\ 93.90\%\pm1.64\%\\ 98.98\%\pm1.20\%\\ 93.79\%\pm1.71\%\\ 92.68\%\pm0.93\%\\ 92.96\%\pm0.87\%\\ \end{array}$	$\begin{array}{c} 96.35\% \pm 1.34\% \\ 91.43\% \pm 2.12\% \\ 96.79\% \pm 1.25\% \\ 91.09\% \pm 2.23\% \\ 88.64\% \pm 0.87\% \\ 90.03\% \pm 0.96\% \end{array}$	$\begin{array}{c} 96.42\%\pm1.36\%\\ 90.78\%\pm2.42\%\\ 96.56\%\pm1.23\%\\ 91.21\%\pm1.98\%\\ 89.44\%\pm0.82\%\\ 90.15\%\pm0.95\% \end{array}$	95.38%±1.46% 90.67%±2.45% 96.10%±1.67% 91.45%±2.06% 89.65%±0.81% 89.34%±0.99%

Sensitive analysis. To evaluate the stability and sensitivity of our TCNN, we implement experiments with different enhanced or noisy datasets to obtain multiple average accuracy values to calculate the variance of them after the model converge to evaluate the stability of the model. The results are shown in the table 6, which showcases the high stability and low sensitivity of our TCNN.

Case study. In addition, as the residual circuit model in the previous work demonstrate unique robustness to adversarial noise attack (Chen et al. 2024), we also conduct experiments to validate its robustness to random noise parameter attacks. Table 4 and 5 separately showcase the average accuracy values and the loss values of the four models. They indicate that the accuracy of the MLP, HFTNN, FATTNN, QiMLP and the two convolutional networks remains about 20%, while the loss values of them rises a lot, finally reaching nan in the program codes, which implies that they are not capable of resisting noise attacks. Since HQNet and HFCNN contains circuit models that could resist noise attacking, they are able to learn features but with lower accuracy than TCNN. Table 6 demonstrates the infinite gradients of the loss function to the attacked parameters of the compared models, which indicates that gradient explosion results in the failure of the model testing. There are more advantageous results about robustness of our TCNN in comparison with the two convolutional networks in the supplementary material.

Ablation study. As we devise paralleled circuit models

with activations and information fusion layer to enhance its performance, we conduct ablation study comparing TCNN and another three hybrid tensor circuit networks (TCNN2, TCNN3 and TCNN4) whose architectures are almost the same as TCNN. TCNN2 possess paralleled circuit framework and information fusion layer but no activation. TCNN3 possess information fusion layer but it only has serial activated circuit framework. TCNN4 possess activation and paralleled circuit architectures but no information fusion layer. The accuracy values on different datasets are shown in table 7. It indicates the importance of the parallelism and activation in the circuit model and the information fusion layer.

Conclusion and discussion

In this paper, we propose a tensor circuit neural network (TCNN) consisting of a tensor neural network with MPO factorization method and paralleled residual circuit models with unitary evolutions and activations. By analyzing its framework and parameter complexity, one advantage of TCNN lies in its low parameter complexity. What's more, groups of experiments demonstrate that TCNN possess more superiority than the MLP, QiMLP, FATTNN, HQNet, HFTNN, HFCNN and two convolutional networks on image classification tasks with clean, enhanced and noisy datasets. In the meantime, the time complexity of TCNN is lower than that of HFCNN and comparable to the MLP and FATTNN. More significantly, groups of case study demonstrate

that our TCNN surpasses other compared models a lot in resistance to random noise parameter attacks due to its distinguished ability to prevent gradient explosion. Meanwhile, our TCNN shows higher stability and lower sensitivity than the compared models. Finally, through an ablation study, we evaluate the advantage of the parallelism, activation operation in the circuit models and the information fusion layer in TCNN. On the basis of these comprehensive strengths, it makes sense to assess TCNN on complicated industrial scenarios with the interference of assorted noises and deploy it on practical electrical hardware to accelerate its industrialization (Kaveh 2024; Xiao et al. 2024).

References

- Bañuls, M. C. 2023. Tensor network algorithms: A route map. *Annual Review of Condensed Matter Physics*, 14(1): 173–191.
- Bies, C. H. H., David A.; and Howard, C. Q. 2017. *Engineering Noise Control*. CRC Press.
- Buduma, N.; Buduma, N.; and Papa, J. 2022. *Fundamentals of deep learning*. O'Reilly Media, Inc.
- Chen, A.; Yin, H.-L.; Chen, Z.-B.; and Wu, S. 2024. Hybrid Quantum-inspired Resnet and Densenet for Pattern Recognition. *arXiv preprint arXiv:2403.05754*.
- Chien, J.-T.; and Bao, Y.-T. 2017. Tensor-factorized neural networks. *IEEE transactions on neural networks and learning systems*, 29(5): 1998–2011.
- Chiribella, G.; D'Ariano, G. M.; and Perinotti, P. 2008. Quantum circuit architecture. *Physical review letters*, 101(6): 060401.
- Chou, Y.-H.; Kuo, S.-Y.; Jiang, Y.-C.; Wu, C.-H.; Shen, J.-Y.; Hua, C.-Y.; Huang, P.-S.; Lai, Y.-T.; Tong, Y. F.; and Chang, M.-H. 2022. A novel quantum-inspired evolutionary computation-based quantum circuit synthesis for various universal gate libraries. In *Proceedings of the Genetic and Evolutionary Computation Conference Companion*, 2182–2189.
- de Sousa Ribeiro, M.; and Leite, J. 2021. Aligning artificial neural networks and ontologies towards explainable AI. In *Proceedings of the AAAI Conference on Artificial Intelligence*, volume 35, 4932–4940.
- Deng, L. 2012. The mnist database of handwritten digit images for machine learning research [best of the web]. *IEEE* signal processing magazine, 29(6): 141–142.
- Dos Martires, P. Z. 2024. Probabilistic neural circuits. In *Proceedings of the AAAI Conference on Artificial Intelligence*, volume 38, 17280–17289.
- Evenbly, G. 2017. Algorithms for tensor network renormalization. *Physical Review B*, 95(4): 045117.
- Fan, Z.; Zhang, J.; Zhang, P.; Lin, Q.; and Gao, H. 2024. Quantum-inspired neural network with runge-kutta method. In *Proceedings of the AAAI Conference on Artificial Intelligence*, volume 38, 17977–17984.
- Fishman, M.; White, S.; and Stoudenmire, E. M. 2022. The ITensor software library for tensor network calculations. *SciPost Physics Codebases*, 004.

- Gao, Z.-F.; Cheng, S.; He, R.-Q.; Xie, Z.-Y.; Zhao, H.-H.; Lu, Z.-Y.; and Xiang, T. 2020. Compressing deep neural networks by matrix product operators. *Physical Review Research*, 2(2): 023300.
- Goodfellow, I.; Bengio, Y.; and Courville, A. 2016. *Deep learning*. MIT press.
- Hameed, M. G. A.; Tahaei, M. S.; Mosleh, A.; and Nia, V. P. 2022. Convolutional neural network compression through generalized kronecker product decomposition. In *Proceedings of the AAAI Conference on Artificial Intelligence*, volume 36, 771–779.
- He, Z.; Deng, M.; Zheng, S.; Li, L.; and Situ, H. 2024. Training-free quantum architecture search. In *Proceedings of the AAAI conference on artificial intelligence*, volume 38, 12430–12438.
- Heidari, M.; Grama, A.; and Szpankowski, W. 2022. Toward physically realizable quantum neural networks. In *Proceedings of the AAAI Conference on Artificial Intelligence*, volume 36, 6902–6909.
- Hendrycks, D.; and Dietterich, T. 2019. Benchmarking neural network robustness to common corruptions and perturbations. *arXiv preprint arXiv:1903.12261*.
- Hendrycks, D.; Zhao, K.; Basart, S.; Steinhardt, J.; and Song, D. 2021. Natural adversarial examples. In *Proceedings of the IEEE/CVF Conference on Computer Vision and Pattern Recognition*, 15262–15271.
- Ji, X.; Liu, Q.; Huang, S.; Chen, A.; and Wu, S. 2024. Quantum sparse coding and decoding based on quantum network. *Applied Physics Letters*, 125(10).
- Kashif, M.; and Al-Kuwari, S. 2024. ResQNets: a residual approach for mitigating barren plateaus in quantum neural networks. *EPJ Quantum Technology*, 11(1): 4.
- Kaveh, A. 2024. Applications of artificial neural networks and machine learning in civil engineering, volume 1168. Springer.
- Li, T.; Xu, X.-Y.; Ding, C.; Tian, T.-C.; Liao, W.-Y.; Zhang, S.; and Huang, H.-L. 2025. AI-Powered Algorithm-Centric Quantum Processor Topology Design. In *Proceedings of the AAAI Conference on Artificial Intelligence*, volume 39, 442–450.
- Li, Z.; Liu, F.; Yang, W.; Peng, S.; and Zhou, J. 2021. A survey of convolutional neural networks: analysis, applications, and prospects. *IEEE transactions on neural networks and learning systems*, 33(12): 6999–7019.
- Liang, Y.; Peng, W.; Zheng, Z.-J.; Silvén, O.; and Zhao, G. 2021. A hybrid quantum–classical neural network with deep residual learning. *Neural Networks*, 143: 133–147.
- Marinov, C. A.; and Neittaanmäki, P. 2012. *Mathematical models in electrical circuits: theory and applications*, volume 66. Springer Science & Business Media.
- Milletari, F.; Navab, N.; and Ahmadi, S.-A. 2016. V-net: Fully convolutional neural networks for volumetric medical image segmentation. In 2016 fourth international conference on 3D vision (3DV), 565–571. Ieee.

- Mitarai, K.; Negoro, M.; Kitagawa, M.; and Fujii, K. 2018. Quantum circuit learning. *Physical Review A*, 98(3): 032309.
- Neill, J. O. 2020. An overview of neural network compression. *arXiv preprint arXiv:2006.03669*.
- Noh, D.-I.; Jeong, S.-G.; and Hwang, W.-J. 2025. Hybrid Quantum ResNet for Time Series Classification. *IEEE Transactions on Emerging Topics in Computing*.
- Ouerfelli, M.; Tamaazousti, M.; and Rivasseau, V. 2022. Random tensor theory for tensor decomposition. In *Proceedings of the AAAI Conference on Artificial Intelligence*, volume 36, 7913–7921.
- Panagakis, Y.; Kossaifi, J.; Chrysos, G. G.; Oldfield, J.; Nicolaou, M. A.; Anandkumar, A.; and Zafeiriou, S. 2021. Tensor methods in computer vision and deep learning. *Proceedings of the IEEE*, 109(5): 863–890.
- Popa, C.-A. 2014. Enhanced gradient descent algorithms for complex-valued neural networks. In 2014 16th International Symposium on Symbolic and Numeric Algorithms for Scientific Computing, 272–279. IEEE.
- Rudolph, M. S.; Miller, J.; Motlagh, D.; Chen, J.; Acharya, A.; and Perdomo-Ortiz, A. 2023. Synergistic pretraining of parametrized quantum circuits via tensor networks. *Nature Communications*, 14(1): 8367.
- Shin, H.-C.; Roth, H. R.; Gao, M.; Lu, L.; Xu, Z.; Nogues, I.; Yao, J.; Mollura, D.; and Summers, R. M. 2016. Deep convolutional neural networks for computer-aided detection: CNN architectures, dataset characteristics and transfer learning. *IEEE transactions on medical imaging*, 35(5): 1285–1298.
- Stokes, J.; Izaac, J.; Killoran, N.; and Carleo, G. 2020. Quantum natural gradient. *Quantum*, 4: 269.
- Wang, A.; Mao, D.; Li, X.; Li, T.; and Li, L. 2025. HQNet: A hybrid quantum network for multi-class MRI brain classification via quantum computing. *Expert Systems with Applications*, 261: 125537.
- Wang, M.; Pan, Y.; Xu, Z.; Yang, X.; Li, G.; and Cichocki, A. 2023. Tensor networks meet neural networks: A survey and future perspectives. *arXiv preprint arXiv:2302.09019*.
- Xiao, H.; Rasul, K.; and Vollgraf, R. 2017. Fashion-mnist: a novel image dataset for benchmarking machine learning algorithms. *arXiv preprint arXiv:1708.07747*.
- Xiao, L.; Zhang, Z.; Huang, K.; Jiang, J.; and Peng, Y. 2024. Noise optimization in artificial neural networks. *IEEE Transactions on Automation Science and Engineering*.
- Yao, J. 2024. Hybrid Tensor Networks: The Integration of Quantum and Classical Machine Learning. In 2024 2nd International Conference on Computer, Vision and Intelligent Technology (ICCVIT), 1–5. IEEE.
- Yin, M.; Phan, H.; Zang, X.; Liao, S.; and Yuan, B. 2022. Batude: Budget-aware neural network compression based on tucker decomposition. In *Proceedings of the AAAI Conference on Artificial Intelligence*, volume 36, 8874–8882.
- Zhang, J.; Wang, T.; Zhang, Z.; Yan, P.; and Li, X. 2025. QiMLP: Quantum-inspired Multilayer Perceptron

- with Strong Correlation Mining and Parameter Compression. In *Proceedings of the AAAI Conference on Artificial Intelligence*, volume 39, 22452–22460.
- Zheng, Y.-B.; Huang, T.-Z.; Zhao, X.-L.; Zhao, Q.; and Jiang, T.-X. 2021a. Fully-connected tensor network decomposition and its application to higher-order tensor completion. In *Proceedings of the AAAI conference on artificial intelligence*, volume 35, 11071–11078.
- Zheng, Y.-B.; Huang, T.-Z.; Zhao, X.-L.; Zhao, Q.; and Jiang, T.-X. 2021b. Fully-connected tensor network decomposition and its application to higher-order tensor completion. In *Proceedings of the AAAI conference on artificial intelligence*, volume 35, 11071–11078.
- Zhou, G.; Han, Y.; and Yu, X. 2025. Factor Augmented Tensor-on-Tensor Neural Networks. In *Proceedings of the AAAI Conference on Artificial Intelligence*, volume 39, 22928–22936.
- Zhou, Z.-H. 2021. Machine learning. Springer nature.